

An Empirical Study of the Nuclear Explosion-Induced Lightning Seen on IVY-MIKE

J. D. COLVIN

Los Alamos National Laboratory, Los Alamos, New Mexico

C. K. MITCHELL

E. G. & G. Energy Measurements, Incorporated, Los Alamos, New Mexico

J. R. GREIG,¹ D. P. MURPHY, R. E. PECHACEK, AND M. RALEIGH

Naval Research Laboratory, Washington, D. C.

We report the results of a unique study of the lightninglike phenomena that were seen to accompany the MIKE shot of operation IVY on October 31 1952. MIKE was a thermonuclear surface burst yielding 10.4 MT, which took place on Enewetak Atoll. During the period of approximately 10 ms after detonation, five discrete luminous channels were seen to start from the ground or sea surface at a distance of approximately 1 km from the burst point and to grow up into the clouds. We have reexamined the original photographic records of IVY-MIKE, obtaining effective brightnesses (optical powers per unit length) for the luminous channels at different altitudes as functions of time. The absolute calibration for the MIKE records was deduced by comparison with the photographic records of other events of that era, laboratory measurements of film sensitivity, and use of atmospheric transmission data taken just prior to the MIKE event. Errors in this analysis lead to an uncertainty of a factor of ~ 2 in the brightnesses of the luminous channels. In the laboratory we have used laser-guided electric discharges to create long (100 cm), arclike plasma channels to simulate the observed luminous channels and to allow determination of an empirical relation between the brightness of the channel and the electric current flowing in the channel. These laboratory discharges had peak currents up to 100 kA and periods of ~ 2 ms. Spectroscopic analysis showed that the luminous channels consisted primarily of normal air plasma with typical ground-level contaminants. Photographic studies showed that these long-duration discharges are unstable to the $m = 1$ magnetohydrodynamic (MHD) instability and become severely distorted in less than 1 ms. By direct comparison of the luminous channels seen at MIKE and the laboratory discharges, we deduce: (1) the peak current in the prominent (brightest) channel at MIKE was between 200 and 600 kA. Here the most likely value of the peak current was 250 ± 50 kA, but potential systematic errors in the film calibration and the comparison of MIKE and laboratory data make higher currents possible. (2) The rapid decline in the brightness of the luminous channels seen at MIKE is caused by a combination of the effects of the MHD instability, which eventually leads to a broadening of the current-carrying channel, and channel cooling by turbulent convective mixing.

1. INTRODUCTION

The MIKE thermonuclear detonation during the IVY U.S. atmospheric test series induced luminous discharges in the vicinity of the detonation. Because of the similarity in appearance between these discharges and natural lightning, the discharges have been called nuclear explosion-induced lightning (NEIL) by previous authors [Longmire, 1978; Uman *et al.*, 1972; Hill, 1973]. Any model for the development, growth, and brightness morphology of NEIL must depend on the spatial and temporal behavior of the electric fields in the vicinity of the detonation and must be able to predict the current carried in the lightning channel. Thus a knowledge of the electric field and current behavior is important to a clear understanding of the physical mechanisms responsible for NEIL, its physical characteristics, and how it differs from natural lightning. In this paper we determine the current in NEIL.

The basic mechanism for the electric field generated in the air by a nuclear detonation was first discussed quantitatively in the open literature by Kompaneets [1958] and corrected by Gilinsky [1965]. Both authors derived an expression for the radial electric field starting with the gamma flux from the explosion. The radially directed prompt gamma flux, with a rise time of a few nanoseconds, produces a radially directed current by Compton interactions with the electrons attached to air molecules. Each Compton electron has an energy of ~ 1 MeV and produces some 3×10^4 secondary electrons by collision. Since the flux of gammas decreases with distance r from the source as e^{-r}/r^2 , the Compton current density also has a radial dependence, and a radial electric field is established. The radial field remains approximately constant with r because a balance is established rapidly between the outward flow of the primary Compton electrons and the inward flow of the secondary electrons in the resulting field; as the air conductivity decreases because the secondary electrons attach (principally to O_2), the primary current also decreases. Creation of gammas by capture in air of the later-time neutrons from the bomb means that the Compton current, the electric fields, and the lightning channels persist for a few tens of milliseconds. Consideration of the conducting ground for sur-

¹ Now at G-T Devices, Alexandria, Virginia.

Copyright 1987 by the American Geophysical Union.

TABLE 1. Camera and Film Data for the Two Film Records That Were Analyzed Radiometrically

Data	Film Record	
	16101	16110
Film type	Microfile	Microfile
Camera focal length, mm	102	25
Timing marks, Hz	No	200
Speed at zero, Frames s ⁻¹	2446*	2560
Exposure duration, μ s	70	78
Effective, f/	4	5.6
Color filter	W-12	W-12
ND Filter	No	No
Developer	D-76	D-76
Development Time	1 min 50 s	4 min 30 s
Development temperature, °F	73°	73°
Film gamma (diffuse density)	0.98	1.45
Step wedge	Yes	Yes
Range, km	34.7	5.9

*There are no timing markers on this record; film speed was determined from measurements of fireball growth versus time.

face bursts forces the initially radial field into a vertical orientation near the ground; indeed, beyond a range of a few hundred meters the tangential component of the field, concentric with the growing fireball, is the dominant field component. The details of the field configuration for a surface burst were first derived by Longmire [1978], who also pointed out that the induced lightning channels followed the tangential field.

Uman *et al.* [1972] were the first to do any quantitative analysis of NEIL, determining from photographic records of the MIKE detonation the upward velocity of the tips of the five lightning channels. They noted that the radial field approximately 1 km from the burst is about 2 orders of magnitude lower than the avalanche value in air ($\sim 2 \times 10^6$ V m⁻¹) and thus infer that the lightning must have initiated on tall metal structures that concentrate the electric field. They also infer from the similarity of NEIL to the upward propagating positive leaders of natural lightning that each NEIL channel carried a current of more than 100 A. Hill [1973] later corrected the Uman *et al.* work to calculate the amplitude of the tangential field at 900 m from the MIKE explosion (the dominant field component at this range) and got essentially the same number ($E \sim 2 \times 10^4$ V m⁻¹) that Uman *et al.* derived for the radial-saturated field. Hill also considered a current of about 100 A per NEIL channel.

In a theoretical model for NEIL described recently by Gardner *et al.* [1984], NEIL is perceived as the glow-to-arc transition for the current that flows to ground in the preionized atmosphere around the nuclear burst as the Compton charge is dissipated. Thus in a glow discharge of ~ 1 A m⁻² sustained by the continuing gamma flux, if current becomes more concentrated in one place, the conductivity there rises, distorting the local electric field and concentrating the current more. This new theory is consistent with the measured upward velocity of the luminous channels but predicts much larger currents in the channels than might be expected of positive leaders, since large fractions of the Compton charge are predicted to flow in each channel [Fernsler, 1985].

We have derived an absolute calibration for the photographic records of the MIKE event and, from these calibrations and the original data records, we have determined the absolute optical power per unit length of lightning channels

radiated in the wavelength band pass of the photo-recording system. In the laboratory we have simulated high-current NEIL discharges and have derived an empirical relationship between current and optical power per unit length. Combining the results of these two independent studies, we infer current levels for the NEIL at the MIKE detonation.

We find that for the lightning channels seen on MIKE the brightness in the wavelength band 5000–7000 Å rises to a peak of a few times 10^7 W m⁻¹ between 5 and 10 ms, then declines to near-background level in about 10 ms. Comparing with our laboratory discharge data, we deduce peak NEIL discharge currents of a few hundred kiloamperes. The uncertainty in the NEIL discharge current of approximately a factor of 3 arises from the difference between the spectral sensitivity of the laboratory photo system and that used in the atmospheric tests and from our inability to accurately extrapolate the laboratory data to the NEIL conditions, both in terms of the absolute brightness and in terms of allowing for the different time history of the NEIL discharges.

2. ANALYSIS OF ATMOSPHERIC TEST DATA

2.1. Description of the Data

We did an absolute radiometric analysis of the induced lightning observed in photographic film records of the Pacific nuclear weapon test IVY-MIKE. These film records were obtained using Eastman high-speed framing cameras fielded by E. G. & G., Incorporated, in support of the Los Alamos National Laboratory. The Eastman framing cameras all used Wratten-12 filters to provide a short-wavelength cutoff of 5000 Å and Kodak Microfile film with an upper wavelength cutoff of 7000 Å. Nominal speeds were 2500 frames s⁻¹, with frame exposure times of approximately 75 μ s. Pertinent camera and film data are summarized in Table 1.

IVY-MIKE was a 10.4-MT thermonuclear explosion that took place on Elugelab Island at the north end of Enewetak Atoll on the morning of October 31, 1952 (local time). One camera station set up to record the event was located on Parry Island, about 35 km across the lagoon to the southeast from the burst. Since this was the first test of a thermonuclear device, there was concern about it not achieving its full design yield, so another camera station was established on Engebi Island, 5.92 km east of the burst location. The film records from the Parry Island station show a total of five lightning channels, three of which provided good time-dependent data and two of which resulted in film exposures barely discernible above threshold, even over a limited time range. In Figure 1 we show one frame from film record 16101, taken at the Parry Island station at a time near peak lightning brightness. For all lightning channels the lightning is observed to have grown up from the surface until it disappeared into or behind the overlying cloud layer at a height of 500–600 m above the burst. The lightning channels grew approximately concentric with the burst, with some of them showing vertically growing branching near the top. They are visible on the film data for typically a few tens of milliseconds, beginning about 2–8 ms after detonation.

2.2. Calibration and Analysis Procedures

To derive the calibration (H&D) curve for the Parry Island film record of MIKE, we relied on the effective exposure method [Buckner, 1967; Constantine, 1968]. This method uses a step wedge, i.e., a strip of the same batch of film as the data

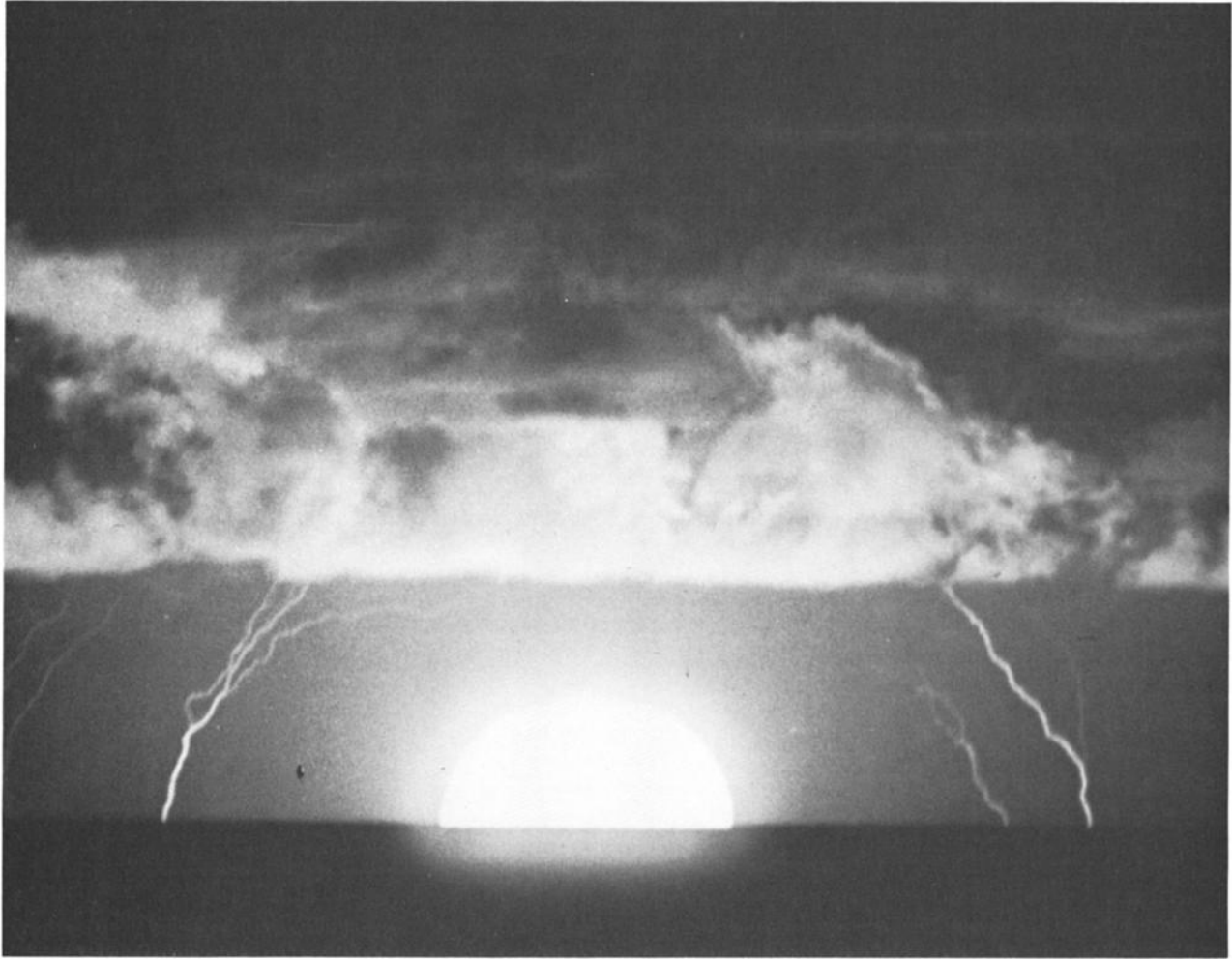


Fig. 1. The MIKE detonation as seen from Parry Island, a distance of 34.7 km from the burst, at 7.4 ms (frame number 18 on film record 16101).

film that has been exposed to a calibrated light source through a stepped sequence of neutral-density filters (a step tablet), then processed in the same way as the data film.

Although a step wedge was available with the Perry Island film record, information about the emissivity of the flash sensitometer used in 1952 to expose this step wedge was not initially available. To overcome this deficiency, we assumed that some old Microfile film in storage at E. G. & G. would have the same sensitivity as the 1950s vintage emulsion. We used a flash sensitometer of known spectral emissivity to expose a strip of old Microfile emulsion through a Wratten-12 filter to make another step wedge and then processed the new step wedge to yield a processing control curve (diffuse density of the film versus transmission of each step of the step tablet), with a gamma (slope) the same as the gamma of the processing control curve of the original step wedge. Then we could match the two processing control curves and obtain the exposure for each step i of the MIKE step wedge as

$$E_i^{(M)} = E_i^{(N)} + \Delta E_i \quad (1)$$

where $E_i^{(M)}$ is the exposure of step i of the original MIKE step wedge,

$$E_i^{(N)} = \int_0^\infty u(\lambda) T_i(\lambda) T_{fil}(\lambda) S(\lambda) d\lambda \quad (2)$$

and ΔE_i is the exposure offset between the i th steps on the two step wedges, which can be calculated from the different transmissions of step i on each step wedge. In (2) $u(\lambda)$ is the spectral emissivity of the sensitometer lamp (in ergs per square centimeter per angström); $T_i(\lambda)$ is the dimensionless transmittance of the i th step of the steptablet; $T_{fil}(\lambda)$ is the dimensionless transmittance of the Wratten-12 filter; and $S(\lambda)$ is the dimensionless spectral sensitivity of the film. This is the preferred procedure for obtaining a H&D calibration because it yields directly an absolute calibration for every step of the step wedge while holding constant the other factors that affect the calibration, namely, the film sensitivity and the processing conditions. In this case, however, we could not be sure that the absolute sensitivity of the Microfile film used to create the step wedge is the same as that of the original data film. Thus we checked this assumption by deriving the calibration in an independent way. It is clear that an absolute H&D calibration can also be obtained if one knows the absolute spectral sensitivity of the data film at a particular photographic density and for given processing conditions. We were able to obtain an absolute spectral sensitivity curve for the old Microfile emulsion. We also obtained archival film-processing data (unpublished) showing the sensitivity of Microfile film relative to that of several other emulsions, including Tri-X, that were measured in 1952. Mitchell *et al.* [1984] performed several labora-

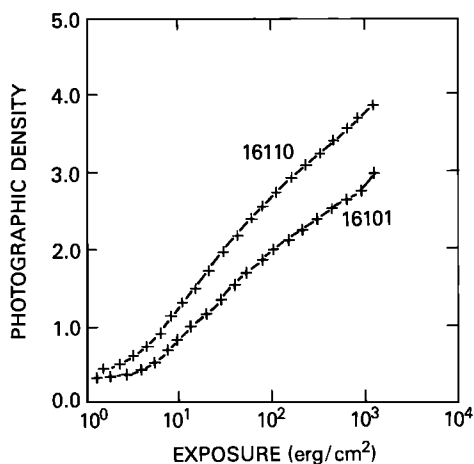


Fig. 2. The H&D calibration curves for MIKE film records 16101 and 16110. The points correspond to the densities of each step of the step wedge, and the curve is a polynomial fit to these points.

tory tests on modern Tri-X film to correct and confirm the Microfile absolute spectral sensitivity. They show that for light in the wavelength interval 5000–7100 Å, an exposure of 5.8 ergs cm⁻² was required to give diffuse density 0.3 above fog on the 1950s vintage Microfile emulsion, when processed in D-76 developer at 75°F for 1 min 30 s. This exposure value can be adjusted for any other processing condition using known time-temperature-gamma relationships for Microfile [Carrol, 1965]. Thus given a processing control curve for any 1950s Microfile step wedge, an absolute H&D calibration can be obtained by fixing the absolute exposure at 0.3 diffuse density above fog. In this way we were able to determine that the older emulsion is approximately 4.5 times more sensitive than the newer one we used to make the calibrated step wedge. This finding is consistent with information we received from the Kodak Company (manufacturers of the Microfile emulsion) that they gradually reduced the silver halide content in several of their emulsions over several years (because of the escalating cost of silver). Accordingly, we used the absolutely calibrated step wedge to derive the H&D calibration in the manner described above and then adjusted it to account for the different sensitivities of the step wedge and data film. Using this procedure, we obtained the H&D calibration curve for film record 16101, shown in Figure 2.

Both the step wedges and the data film were digitized on a PDS scanning microdensitometer. The grain size on the Microfile emulsion is ≤ 20 μm . Accordingly, we chose a square microdensitometer scanning aperture 20 μm on a side and a step-over scanning interval of 20 μm to minimize the film grain noise while maximizing the spatial resolution. Thus each pixel on the film corresponds to an image area of 400 μm^2 . For this pixel size the width of the lightning channel images is typically 1–3 pixels. For the 102-mm focal length and 35-km range of the Parry Island camera, 1 pixel width corresponds to ~ 7 m at the source. We do not believe, however, that the NEIL channels are 7 m or more wide. We assume, instead, that all of the source light comes from a channel that is much narrower than 7 m but that the film sees the source radiance averaged over the pixel area. Since the development process develops whole grains, not partial grains, the lightning image will always appear to be 1 or 2 pixels wide, and we assume that where it is wider than 2 pixels we are seeing adjacency or some other development effect that

acts to spread the image on the film. Thus we sum the exposures of all those pixels across the lightning channel that are above background and calculate the source power per unit length as if all the light came from 1 source pixel. We also assume that the source is a Lambertian radiator that emits isotropically into 4π sr. Under these assumptions, one can show that the source brightness (power per unit length in watts per meter) is

$$B = \left[\frac{16(f/l)^2 l}{t_{\text{exp}}} \right] \left[\frac{\int d\lambda}{\int T_{\text{opt}}(\lambda) T_{\text{fil}}(\lambda) T_{\text{atm}}(\lambda) S(\lambda) d\lambda} \right] \sum_i E_i \quad (3)$$

where f/l is the focal ratio and t_{exp} the exposure time in seconds (see Table 1), l is the length in meters of 1 pixel at the source, E_i is the exposure for pixel i in joules per square meter, and the sum is taken over all those pixels across the lightning channels that are above background.

A total of 36 data frames were digitized from the Parry Island record, covering the time range during which the lightning was visible. A computer code scanned each horizontal scan line in the digital image, masked to include just the area around an individual channel, and selected the position of the maximum digital density in the scan line as the position of the channel center. Then, proceeding out from this center position in both directions, the routine counted all pixels with density above a threshold density as belonging to the channel. The threshold density was set at three standard deviations above the background density, where the background density at each point along the scan line was calculated from the coefficients determined in a linear least squares fit of all the density points (except the one at channel center and a few on each side of center) versus position in the masked portion of the scan line. Each pixel density so included in the lightning channel was converted to exposure, using Figure 2, and the brightness at that channel position was computed from (3).

In order to apply (3) we need to know all the spectral transmissions between the film and the source, including the atmospheric transmission, $T_{\text{atm}}(\lambda) = \exp[-\sigma_T(\lambda)R]$. The total extinction coefficient σ_T for the atmosphere consists of two parts: one resulting from Rayleigh scattering, and the dominant one at sea level resulting from aerosol extinction, which is approximately spectrally flat over the optical wavelength interval of interest. There is no information available on the visibility range (distance at which the transmission is 0.02 for $\lambda = 5500$ Å) at Enewetak Atoll for the day of the MIKE detonation. Instead, we depended on some transmissometer measurements made just before the event by the Naval Research Laboratory (NRL) team under the direction of Harold Stewart and reported by Wilson [1980]. The air transmission resulting from these measurements was used in calculating the product of transmissions and sensitivity in the integral in the denominator of (3). This product as a function of wavelength is shown in Figure 3. The sharp cutoff at 5000 Å is defined by the Wratten-12 filter, and the sharp cutoff at 7100 Å is where the film sensitivity goes to zero.

Although we have no reason to believe that the NRL transmissometer measurements were incorrect or that the numbers were incorrectly reported, the measurements do imply a visibility range that is unusually high (67.4 km) for a subtropical maritime atmosphere: $\sigma_T(\lambda = 5500 \text{ Å}) = 0.058 \text{ km}^{-1}$. Indeed, a review of the available atmospheric transmission data (trans-

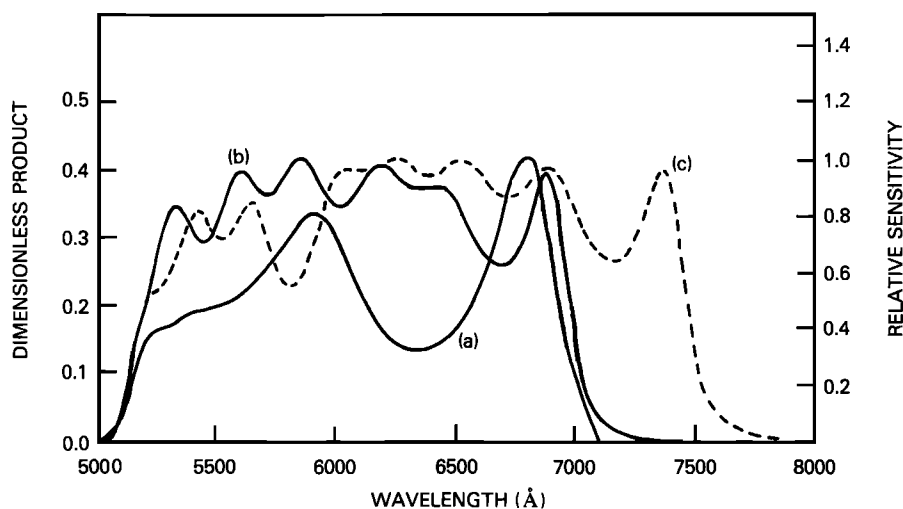


Fig. 3. (a) The dimensionless product of the spectral sensitivity of the Microfile film and the spectral transmissions of the Wratten-12 filter, the camera lens, and atmosphere versus wavelength (scale on left). (b) Relative sensitivity of the LS-700 filter with a Wratten-12 filter. (c) Relative sensitivity of the LS-750 filter with a Wratten-12 filter. (For Figures 3b and 3c, refer to scale on right.)

missometer measurements and visibility ranges) for other events at Enewetak and Bikini Atolls yields σ_T ($\lambda = 5500$ Å) = 0.16 ± 0.05 km⁻¹, corresponding to visibility ranges of $24.4^{+11.2}_{-5.8}$ km (see, for example, Curcio *et al.* [1953]).

One should note, however, that transmissometer measurements, made for a few events along a slant path 91.4 m high to near sea level over a slant range of 3.66 km, gave visibility extinction coefficients half the 2-m-high horizontal path measurements. The Eastman cameras on Parry Island that obtained the MIKE data reported here were fielded on towers at a height of 22.9 m (i.e., 75 feet). Although, in principle, one should allow for the altitude dependence of atmospheric extinction coefficients, we did not do so in the present analysis.

For an uncertainty of $\Delta\sigma_T$ in the total atmospheric extinction coefficient, the fractional uncertainty in the air transmission is

$$\frac{\Delta T_{\text{atm}}}{T_{\text{atm}}} = R \Delta \sigma_T \quad (4)$$

Thus at large range, even a modest uncertainty in σ_T implies a large uncertainty in air transmission. For the Parry Island record of MIKE, if $\Delta\sigma_T = 0.05$, the fractional uncertainty in the air transmission is 175%! If the visibility was, in fact, worse than the NRL transmissometer measurements imply, then the lightning brightnesses derived from the Parry Island film record could be too low by as much as a factor of 6!

This large uncertainty compelled us to analyze a film record taken at the close-in station on Engebi Island. The much smaller range implies a smaller uncertainty in the air transmission for this record. Both a step wedge and a processing control curve are available for record 16110. The step wedge was exposed through an ND1 filter, a Wratten-12 filter, and with a sensitometer that delivered its energy in a flash time of 500 μs. Both the step wedge and data film were processed in D-76 developer at 73° F for 4 min 30 s (Table 1).

We have already shown above that the absolute spectral sensitivity of the 1950s vintage Microfile emulsion implies that for light in the wavelength interval 5000–7100 Å an exposure of 5.8 ergs cm⁻² is required to give diffuse density 0.3 above fog when the film is processed in D-76 developer at 75°F for 1

min 30 s. This exposure value was adjusted for the processing conditions of record 16110 using the known time-temperature-gamma relationships for Microfile [Carroll, 1965]. Thus an absolute H&D calibration for record 16110 was obtained by using the processing control curve and fixing the absolute exposure at 0.3 diffuse density above fog. In this way we obtained the H&D calibration curve for record 16110 shown in Figure 2. Since some of the specular densities in the lightning data on record 16110 are slightly higher than 3.7, the highest specular density on the step wedge, the H&D curve was extrapolated to density 3.9, corresponding to approximately one step on the wedge. Note that because of the increased processing time, 4 min 30 sec versus 1 min 30 s, less than 5.8 ergs cm⁻² (i.e., 3.5 ergs cm⁻²) were required to produce diffuse density 0.3 above diffuse fog ($D_{\text{fog}} = 0.26$).

2.3. Results

Figure 4a shows the brightness versus time at 48 m above the base of the brightest NEIL channel seen on MIKE from the Parry Island station (the channel closest to the fireball on the left of Figure 1). Comparing with Figure 4b, which shows brightness versus time for the same NEIL channel at 102 m above the base, it is evident that the NEIL brightness morphology was approximately independent of channel height (except near the tip of the lightning channel). At 48 m above the base the NEIL brightness rose rapidly to a peak of 3.55×10^7 W m⁻¹ at 7.4 ms, then decayed to near background in 10–15 ms. At 102 m above the base the behavior was similar, with the brightness having reached a peak of 5.30×10^7 W m⁻¹ at 5 ms. Within the combined uncertainties the brightness was constant with height (away from the tip) at all times. (We note that we have neglected to correct the brightness for the altitude dependence of atmospheric extinction coefficients. This will tend to decrease the brightness at higher altitudes.)

All five of the NEIL channels seen in the record from the Parry Island station are also seen in the record (16110) from the close-in station. The two brighter ones in the latter record we can unambiguously identify as being the same NEIL channels as the two closest to the fireball on the left in the Parry Island record (Figure 1). For these two channels we list

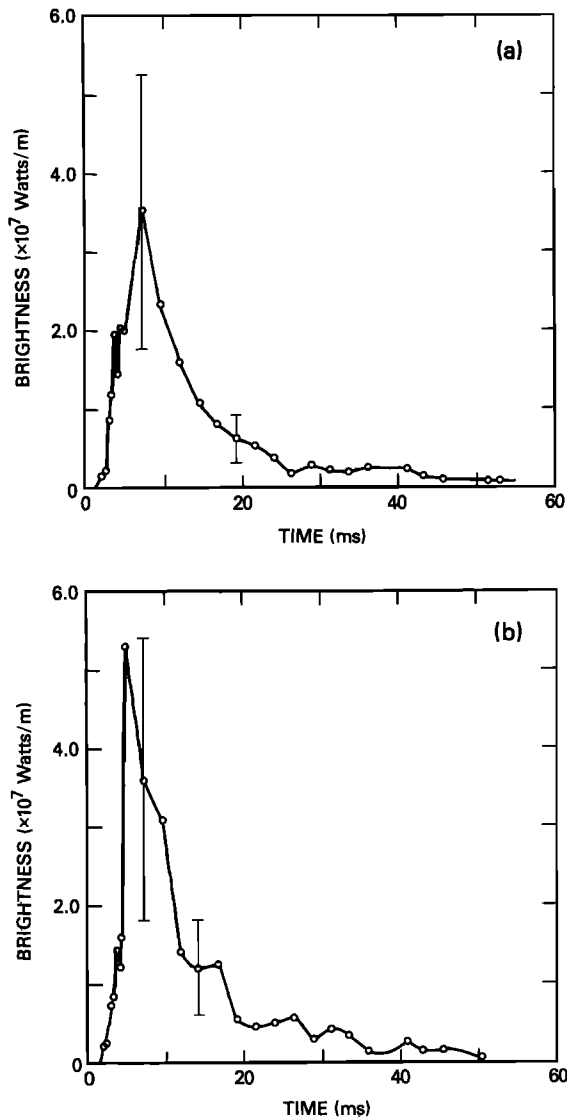


Fig. 4. Brightness versus time of one NEIL channel seen in record 16101 of MIKE (the one closest to the fireball on the left in Figure 1) at (a) 47.6 m and (b) 102.0 m above the base of the channel. The vertical error bars indicate the possible range in brightness accounting for uncertainties in the radiometric analysis, $\pm 50\%$ at all times.

in Table 2 the peak brightness at ~ 50 m above the base, as determined from the different and independent radiometric analyses of the two film records. Clearly, there is good agreement in the results from these two records. Thus we conclude that there is no systematic error introduced by the air transmission.

The other NEIL channels on MIKE had a very similar brightness morphology to that shown in Figure 4; i.e., the brightness rose to a peak of between about 1×10^7 and 1×10^8 W m⁻¹ in less than 10 ms, then fell to near-background brightness in about 10 ms. For a NEIL channel 500 m high this corresponds to a total radiated optical power of $> 10^{10}$ W in the 5000- to 7000-Å wavelength interval.

This brightness and power, and its time duration, are much greater than the corresponding quantities for natural lightning. For example, Guo and Krider [1982] found a mean peak brightness radiated by the first return stroke of Florida lightning of $1 \pm 0.9 \times 10^6$ W m⁻¹, about 4 times larger than the

mean for normal subsequent return strokes. Their measurements were made with a silicon photomultiplier, thus recording light in the 4000- to 11,000-Å wavelength interval. The greatest peak brightness they measured was 5×10^6 W m⁻¹. They also found a mean time to peak brightness of 57 ± 22 μs and a mean peak power radiated by first return strokes of $2.3 \pm 1.8 \times 10^9$ W. The greatest peak power they measured was $\sim 10^{10}$ W. Their values are comparable to those for Florida lightning first return strokes measured earlier by Turman *et al.* [1976] with both silicon and S4 photomultipliers. Turman *et al.* found that 35% of their data for optical power are in the range 1×10^9 to 2×10^{10} W, with the greatest at 2×10^{11} W and most of the strokes reaching peak power before 50 μs. Barasch [1970], also found an average optical power of 4×10^9 W for lightning first return strokes. Turman [1979] found a median optical power of 1×10^9 watts for lightning measured worldwide from satellites. Furthermore, Turman *et al.* [1976] found that the strong spectral lines of neutral oxygen at 7774 Å and of neutral nitrogen at 8683 Å dominate the optical radiation, with approximately 15–20% of the total power in the silicon band contributed by each of these lines. Neither of these lines, or course, was seen by the film that recorded the NEIL data. Thus NEIL is at least 10–100 times brighter than natural lightning (neglecting lightning superbolts [Turman, 1977]) and lasts more than 100 times longer.

2.4. Uncertainties

There are three principal sources of uncertainty in the NEIL brightnesses reported here that arise from the digitizing and calibration procedures. One uncertainty is derived from the uncertainty in the exposure offset (ΔE , in equation (1)) required to match the uncalibrated MIKE processing control curve for record 16101 to the calibrated processing control curve. We estimate that there is about 9% fractional uncertainty in the brightness introduced by the curve-matching procedure. Note that since the calibrations were obtained in a different way for the other film record, this uncertainty applies only to MIKE record 16101.

Another source of uncertainty is in the averaging procedure used to obtain the specular density of each step of the step wedge. The density for each step of the step wedge is the average of the pixel densities in three scan lines across the length of the step. Comparing the three scans for each of the 21 steps in the step wedge of record 16101, we find an average standard deviation of $\Delta D = 0.114$. Thus using $\Delta D = \gamma \Delta \log E$, so that

$$\Delta E = [1 - 10^{-(\Delta D/\gamma)}]E \quad (5)$$

there is about a 21% fractional uncertainty in the brightness.

The third uncertainty is an uncertainty in the individual data densities because of scanning noise in the digitization

TABLE 2. Peak Brightness at ~ 50 m Above the Base for Two NEIL Channels

Channel	Record	
	16101	16110
1	3.55×10^7	6.45×10^7
2	0.65×10^7	0.83×10^7

Brightness is stated in watts per meter.

process. Using (5), we estimate that for record 16101 this introduces about 18% fractional uncertainty in the brightness.

The total uncertainty is the sum of these three, or 48% for record 16101. This uncertainty is indicated in Figure 4. Most of this uncertainty arises from uncertainty in the digitization of both the step wedge and the data film. Accordingly, we sought to improve the digitization for our analysis of the other MIKE record. We estimate that the total fractional uncertainty in brightness introduced by the digitizing and calibration procedures for record 16110 is no more than 20%.

The largest single source of uncertainty in brightness, however, is still the air transmission. The fact that the NEIL brightness determined for the same NEIL channels as seen on record 16101 at 35-km distance and record 16110 at 6-km distance agree to within the combined uncertainties gives us confidence that the air transmission, and hence the absolute brightness, is not grossly wrong. There is, however, still some uncertainty in the total atmospheric extinction coefficients $\Delta\sigma_T$. Where both transmissometer measurements and visibility range estimates were made for Pacific nuclear test events, the visibility range estimate R_v agrees with the visibility range inferred from the transmissometer measurements to within ± 3 nautical miles (± 5.56 km). Then, since $\Delta\sigma_T/\sigma_T \approx \Delta R_v/R_v$, we have $\Delta\sigma_T \approx 0.005 \text{ km}^{-1}$ for MIKE. From (4) this uncertainty in the total extinction coefficient corresponds to 17.5% fractional uncertainty in the air transmission at 35 km and thus to approximately 20% uncertainty in the brightness. This is a relatively small uncertainty, despite the large distance, because the visibility range is exceptionally large (and thus we know it to within 8%).

Overall, then, it is safe to say that we now know the NEIL absolute brightnesses to within a factor of 2, which is smaller than the range of NEIL peak brightnesses we have observed.

3. LABORATORY SIMULATION

3.1. Apparatus for Channel Formation

To make long discharges in the atmosphere that are real air plasmas and are precisely located both in time and in space, we use the technique of laser-guided electric discharges. This technique has been developed at NRL over a period of several years and has been used in a variety of research efforts [Greig *et al.*, 1978, 1982; Murphy *et al.*, 1981].

The path of the laser-guided electric discharge is designated by the beam from a Nd:glass laser. This laser is Q-switched and typically delivers $\sim 100 \text{ J}$ in $\sim 40 \text{ ns}$. The beam is focused by a 5-m focal length lens and the laser-atmosphere interaction is enhanced by the presence either of a water mist produced by a Microsol model 101 mechanical aerosol fog generator (TIFA, Limited, Millington, N. J.) or of a light smoke ($\sim 10^{-7} \text{ gm cm}^{-3}$) which is created by burning a small quantity of black gunpowder (FFFg Superfine Black Rifle Powder, manufactured by GOEX Incorporated, Moosic, Pa.) A compact Marx generator provides a high-voltage discharge, typically $\sim 300 \text{ kV}$, with a peak current of $\sim 10 \text{ kA}$ and a period of $\sim 3 \mu\text{s}$, that tracks the laser-preionized path and decays away in approximately two periods. Once this initial discharge has begun, different auxiliary discharge circuits can be switched in and subsequent discharges will follow the same path. The delay between firing the Nd:glass laser and firing the Marx generator is always $30 \mu\text{s}$, and electric breakdown occurs immediately ($< 100 \text{ ns}$). There is also no breakdown delay when the auxiliary discharge is initiated.

Three separate auxiliary discharges have been studied as simulations for NEIL.

- (1) $C = 8 \mu\text{F}$, $V_{\text{max}} = 50 \text{ kV}$, $Q = 0.4 \text{ C}$, $E = 10 \text{ kJ}$;
- (2) $C = 320 \mu\text{F}$, $V_{\text{max}} = 10 \text{ kV}$, $Q = 3.2 \text{ C}$, $E = 16 \text{ kJ}$;
- (3) $C = 3200 \mu\text{F}$, $V_{\text{max}} = 20 \text{ kV}$, $Q = 64 \text{ C}$, $E = 640 \text{ kJ}$.

Discharge 1 is produced using the circuit shown in Figure 5a. For a charging voltage of 50 kV, peak currents of $\sim 80 \text{ kA}$ are obtained. The detonator-activated, solid dielectric switch S closes $\sim 40 \mu\text{s}$ after the firing of the Marx generator, when the conditions existing in the channel formed by the Marx discharge are varying very slowly. The purpose of this discharge is to demonstrate the effect of very high rates of current rise ($\sim 10 \text{ kA } \mu\text{s}^{-1}$), when pressure equilibrium cannot be maintained. Discharges 2 and 3 are both produced using the circuit shown in Figure 5b. Now there is no delay between the Marx and the auxiliary discharge, and the two currents are simply superimposed. For discharge 2 the inductor value is $80 \mu\text{H}$. The charging voltage is 10 kV, and the peak current is only 16 kA. The discharge period is 1.1 ms, and the discharge damps within two periods. For discharge 3 the charging voltage was either 10 kV or 20 kV, with resulting peak currents of $\sim 50 \text{ kA}$ and $\sim 100 \text{ kA}$, respectively. The total system inductance was $\sim 40 \mu\text{H}$. The nominal period of 2 ms of this system was determined by inserting a copper bar in place of the discharge column and allowing the system to ring. In fact, the discharge column resistance was sufficient to cause a nearly critically damped discharge. For all discharges, the discharge electrodes were spaced 1 m apart when the smoke aerosol was used and 50 cm apart when the water aerosol was used.

3.2. Diagnostic Apparatus

The electric current in the different discharges was measured using a variety of Rogowski coils and Pearson transformers in conjunction with Tektronix oscilloscopes. From current traces, both the inductance and the circuit resistance were derived. For the Marx discharge, half the circuit resistance was in the Marx switches and half in the air column, but for the auxiliary discharges, essentially all the circuit resistance was in the air plasma column.

The time-resolved light emission from the discharge was measured with a Hamamatsu R636 GaAs photomultiplier tube (PMT) (Hamamatsu Corporation, Middlesex, N. J.). This tube has a spectral response that is nearly independent of wavelength from 3000–8000 Å. The light from the discharge passed through several neutral-density filters, a Wratten-12 filter (Eastman Kodak Company, Rochester, N. Y.) and either a Corion LS-700 (Corion Corporation, Holliston, Mass.) or a LS-750 filter before reaching the PMT. The Wratten-12 filter gives our system the same short-wavelength cutoff as the cameras at the IVY-MIKE test. The long-wavelength cutoff in the original camera system was that of the Kodak Microfile film itself, near 7000 Å. To determine how sensitive the measurements are to this long-wavelength cutoff, intensity measurements were made with both the LS-700 and the LS-750 red cutoff filters. Figure 3 shows a comparison of the spectral sensitivity of the Microfile film and Wratten-12 filter to that of the two PMT/filter sets. Note that while there is only a slight difference in the long-wavelength cutoff between the Microfile film and the LS-700 filter, the filter is unable to accurately match the film response between 6000 and 6800 Å, a spectral region which includes the prominent feature H_α at 6563 Å.

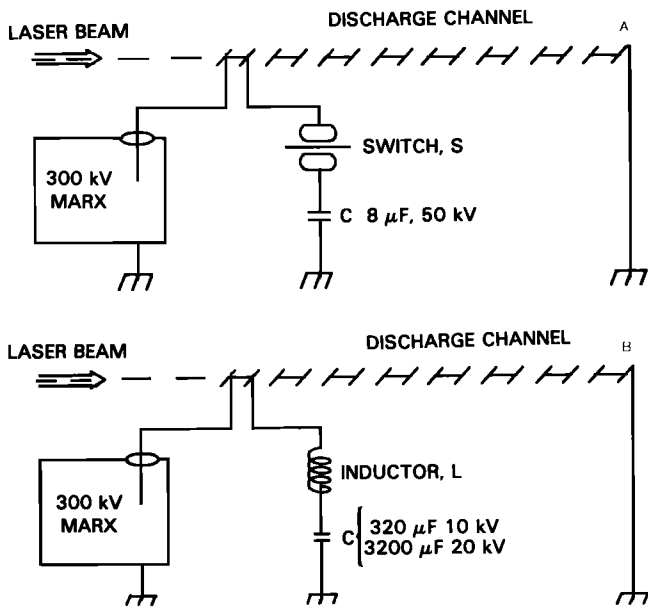


Fig. 5. Schematic diagrams of the apparatus for producing (a) 30- μ s period discharges (capacitor bank 1); and (b) 1- and 2-ms period discharges (capacitor banks 2 and 3).

The absolute sensitivity of each of the PMT/filter combinations was calibrated with a tungsten ribbon reference source which had previously been calibrated by the National Bureau of Standards. The field of view of the PMT included a 27.5-cm-long section of the discharge channel, centered midway between the discharge electrodes, and the width of the field of view was larger than the maximum diameter of the discharge channel (27.5 cm compared to 25 cm for the 100-kA channel).

The geometry of the discharge channel was studied using high-speed framing photography of the white light emitted from the channel. For this, a Cordin 330 camera (Cordin Corporation, Salt Lake City, Utah) with Kodak Tri-X film was used. A front-surfaced mirror was suspended above the channel in the field of view of the camera so that side-on and overhead views were recorded simultaneously.

The geometry of the reduced density channel created by the laboratory discharges was investigated using high-speed framing schlieren photography. The strobe light used to back light the channel was a repetitively pulsed argon ion laser with an integral cavity dumper (Spectra Physics model 165-09) (Spec-

tra Physics Incorporated, Mountain View, Calif.) The camera was an NRL-designed N1C streak camera using Tri-X film [Brauer and Hansen, 1959]. An argon laser line filter was placed in the optical path to prevent white light emitted by the discharge channel from fogging the film.

The detailed structure of the spectrum emitted from the discharges between 3000 and 8800 Å was recorded using a SPEX model 1700 spectrometer (SPEX Industries Incorporated, Metuchen, N. J.), with a 600 lines mm^{-1} grating and entrance slit width of 50 μm . Mercury and argon reference lines were superimposed on the film at shot time to facilitate identification of prominent features on the spectrograms. The SPEX field of view was limited to a very narrow diametric slice of the plasma column midway between the electrodes. Thus the minimum amount of electrode material (mostly Cu and Zn) was able to migrate into the field of view while the channel was still luminous. As a test that the PMT also would see only clean air under normal operating conditions, one of the brass electrodes was moved progressively closer to the spectrometer's field of view. Not until the electrode was within 10 cm of that spot did any significant amount of metal contamination of the plasma column appear on the spectrograms.

3.3. Results

There are four characteristic lengths associated with the discharge column that can be measured from the white light and schlieren photographs (Figure 6): R_f is the radius of the luminous current filament, measured from the white light photographs; R_e is the radius of the envelope of the luminous filament, i.e., the amplitude of the magnetohydrodynamic (MHD) distortions, also measured from the white light photographs; R_d is the radius of the reduced density channel created by the discharge, measured from the schlieren photographs; λ is the average wavelength along the discharge of the MHD distortions, measured from the white light photographs.

White light and schlieren photographs of the fast-ringing 80-kA discharge produced by bank 1 (discharge 1, see section 3.1) show cylindrical profiles that persist throughout the discharge lifetime. Since no MHD distortions are present, the filament radius R_f of ~ 1 cm is equal to the envelope radius R_e . The density channel radius R_d , measured from the schlieren photographs, is ~ 2 cm.

Figure 7 shows selected white light and schlieren photographs of the 16-kA discharge of bank 2. The channel begins life as a straight cylindrical discharge, but from ~ 40 μs , dis-

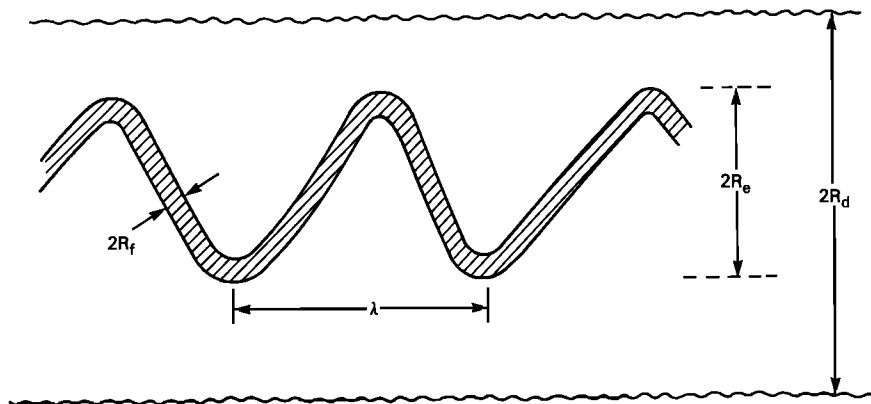


Fig. 6. Characteristic lengths of the discharge column: R_f is the luminous filament radius; R_e is the radius of the envelope of the MHD distorted discharge; R_d is the radius of the reduced density channel around the discharge; λ is the average wavelength of the MHD distortions on the discharge column.

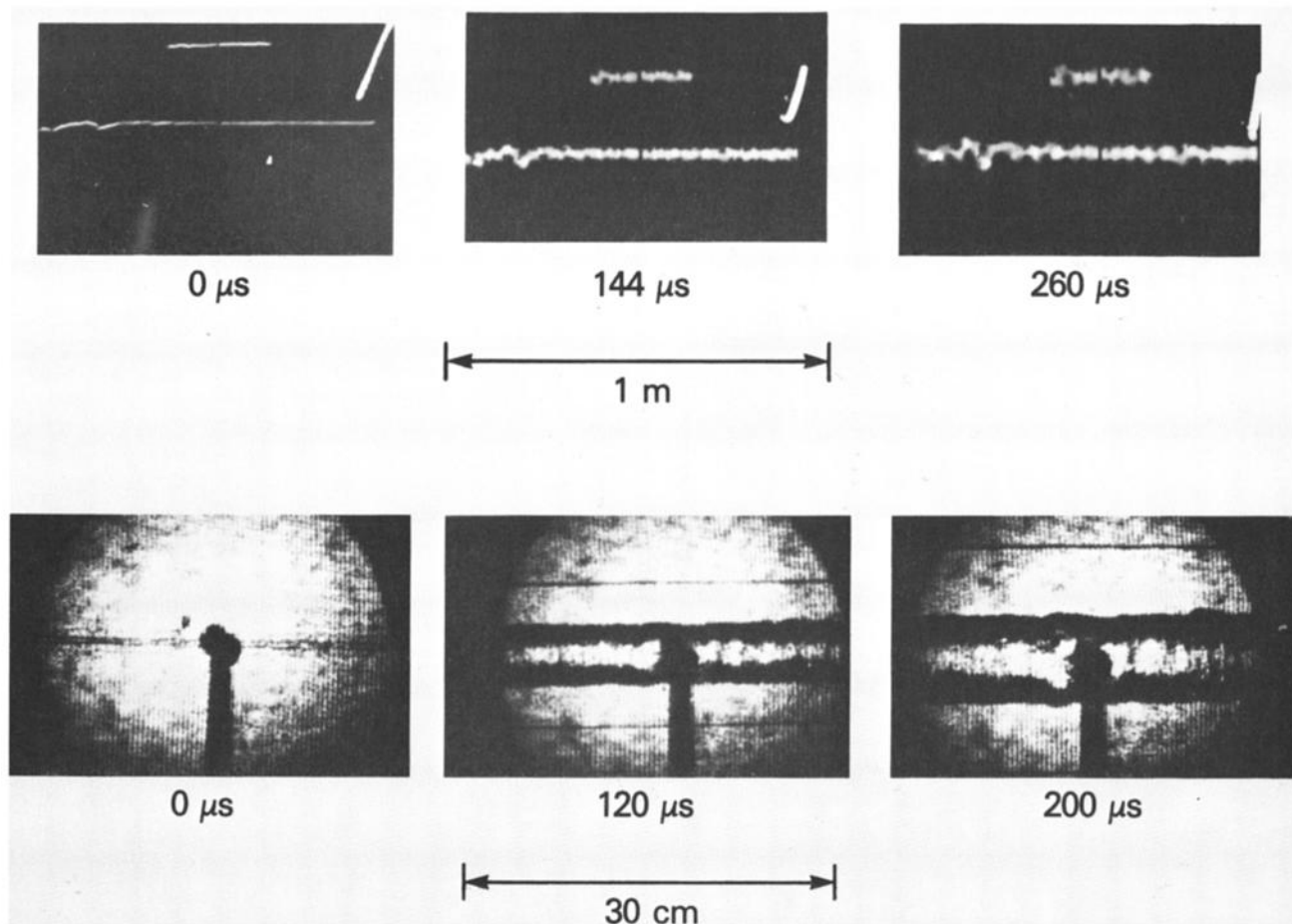


Fig. 7. Selected white light photographs (upper set) and schlieren photographs (lower set) of the discharge column produced by bank 2; peak current = 16 kA, discharge period = 1.1 ms. The exposure time for the white light photographs was 29 μ s. The exposure time for the schlieren photographs was 14 ns. The length scales are shown below each set of photographs, as are the times in microseconds when each photograph was taken.

tortion by MHD instabilities becomes significant. The most rapidly growing instability appears to be the $m = 1$ kink mode [Manheimer *et al.*, 1973]. By approximately 250 μ s, the filament radius is still on the order of 1 cm, but the envelope radius has grown to ~ 3 cm. The average wavelength λ of the distortions has grown to ~ 5 cm and continues to increase with time. The density channel created by the energy deposited in the air grows to a radius R_d of ~ 4 cm and is nearly smooth despite the strongly perturbed luminous channel that resides within it.

Figures 8a and 8d show the white light photographic data for a 50-kA and a 100-kA discharge, respectively, of bank 3. Again, both the amplitude R_e and wavelength λ of the MHD instabilities can be seen to grow with time to ~ 10 cm, even though the filament radius R_f is nearly constant at about 2 cm. The density channel radius R_d does not vary appreciably along the length of the discharge, but it does grow with time to beyond the limit of the schlieren camera's field of view at $R_d = 15$ cm. The full-time variation of the radius data for the 50-kA discharge and the current time history are shown in Figure 9.

In general, for the longer-duration discharges the discharge channel was always in pressure equilibrium with the surrounding atmosphere, and the radius of the luminous current channel was always significantly less than that of the density channel. In fact, although these discharges also started as cyl-

inders, MHD instabilities became a dominant feature of the current channel from about 40 μ s onward. Thus at later times there was a current filament distorted by MHD instabilities whose amplitude was equal to or larger than the radius of the current filament, and this whole current structure resided inside the yet larger radius density channel. The reduced density channel was approximately cylindrical, and the major features of the current channel remained stationary within the density channel. Such a discharge channel inherently has a very nonuniform energy deposition profile and will therefore be cooled by turbulent convective mixing [Picone and Boris, 1983; Greig *et al.* 1985], i.e., mixing into the channel of cold surrounding gas.

The peak current of the discharge produced by bank 1 is ~ 80 kA and the peak brightness, which is not reached until the second half-cycle of the discharge, is 0.8×10^8 W m $^{-1}$ of channel length within the bandwidth of the LS-750 filter set. This discharge rings on a time scale too short for pressure equilibrium to be established with the surrounding atmosphere, thus its brightness is not a simple function of the discharge current.

The peak current for the discharge produced by bank (2), charged to 10 kV, is only 16 kA, with a maximum brightness of 0.6×10^7 W m $^{-1}$. Again, the LS-750 filter set was used for the brightness measurement. In this longer-duration discharge the plasma approaches pressure equilibrium with the sur-

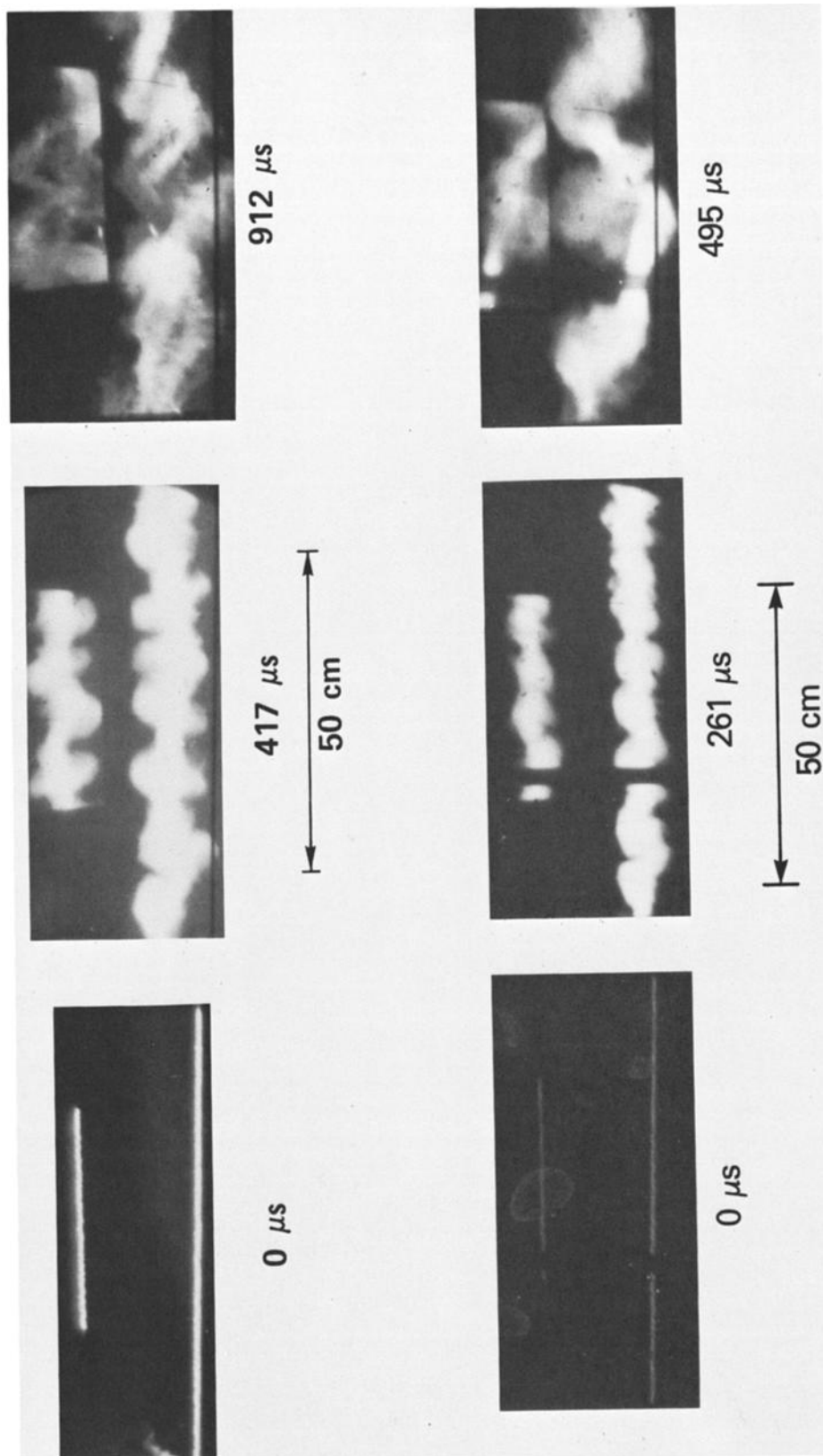


Fig. 8. Selected white light photographs of the discharge column produced by bank 3 (a) charged to 10 kV; peak current = 50 kA, period = 2 ms; and (b) charged to 20 kV; peak current = 100 kA, period = 2 ms. The exposure time for each frame was 26 μ s. The length scales are shown below each set of photographs, as are the times in microseconds when each photograph was taken.

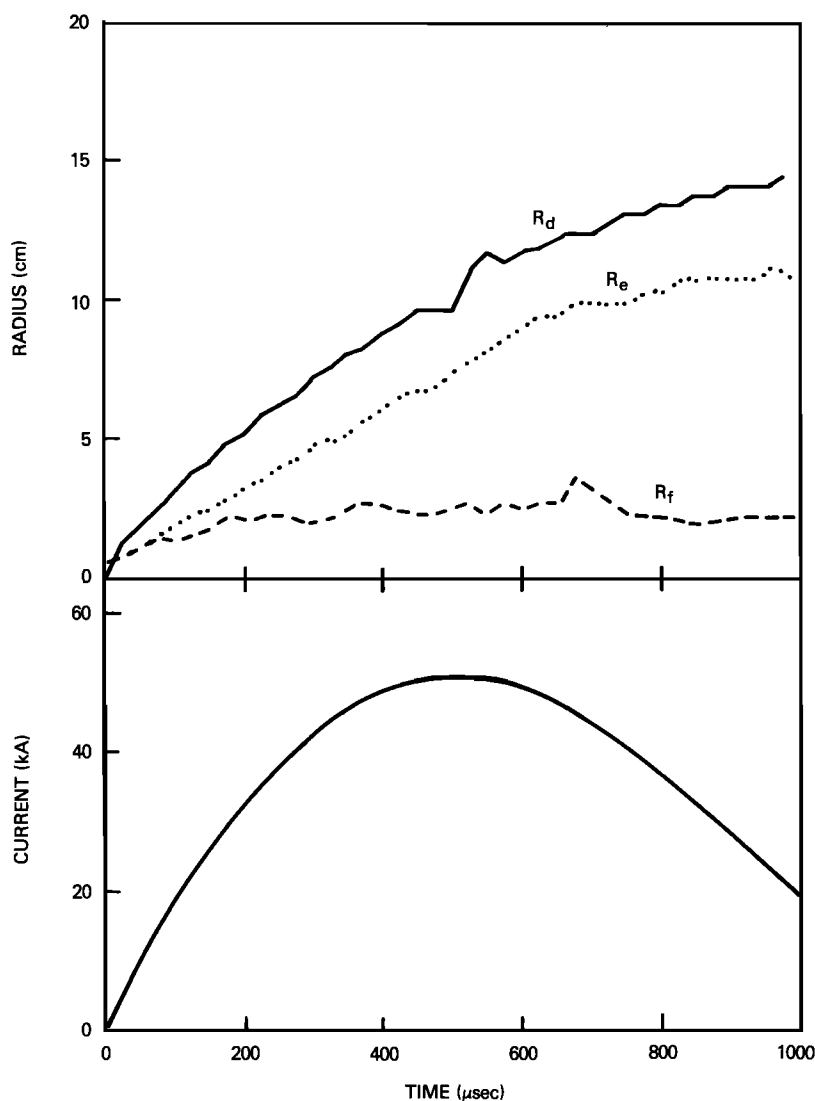


Fig. 9. The time histories of the discharge current and the discharge channel radii, R_f , R_e , and R_d (see Figure 6) for a 50-kA peak current discharge of bank 3.

rounding atmosphere, and the brightness is more nearly a simple function of the discharge current similar to that shown in Figure 10.

For discharges of 50-kA and 100-kA peak current created using bank 3, the brightness was measured using both the LS-700 filter set and the LS-750 filter set. In all cases the brightness was a simple function of the discharge current, as shown in Figure 10, but the difference between measurements with the two filter sets was surprising. Typical discharges with peak currents of ~ 50 kA gave peak brightness of $0.34 \times 10^7 \text{ W m}^{-1}$ with the LS-700 filter set and $0.27 \times 10^8 \text{ W m}^{-1}$ with the LS-750 filter set. Typical discharges with peak currents of ~ 100 kA gave peak brightnesses of $0.85 \times 10^7 \text{ W m}^{-1}$ with the LS-700 filter set and $0.74 \times 10^8 \text{ W m}^{-1}$ with the LS-750 filter set. The reproducibility of these brightness measurements for a given discharge (current) was better than about $\pm 5\%$.

Analysis of the spectra emitted by these discharges revealed a set of strong lines between 7150 and 7500 Å due to neutral oxygen and nitrogen atoms, and both the LS-700 filter set and the Kodak Microfile film cut off below 7150 Å. In contrast to this strong dependence on the long-wavelength cutoff, the

brightness of the discharge channels was independent of the aerosol used to initiate the discharge breakdown, i.e., gunpowder smoke or water mist, though the hydrogen lines are clearly stronger in the spectra of the water-initiated discharges.

Figure 11 is a plot of the brightness versus current for a typical 50-kA shot and for a typical 100-kA shot on bank 3, when the LS-700 filter set was in place on the PMT. A graph very similar to that of Figure 11 was constructed for the LS-750 filter set brightness data from the 16-kA, 50-kA, and 100-kA peak current discharges, the sole distinction being that the brightness scale was increased by about a factor of 8. We note that in Figure 11 the brightness is greater when the current is increasing than when the current subsequently decreases and that the brightness actually begins to decay before peak current is reached at 500 μs . This indicates that the plasma column is cooling despite the rising current, probably because of turbulent convective mixing. It is also consistent with our expectation that there is no steady state equilibrium for these long discharges in the atmosphere and that were continuous wave (cw) current available the discharge channel would become "unstable" and "blow" itself out. A simple qua-

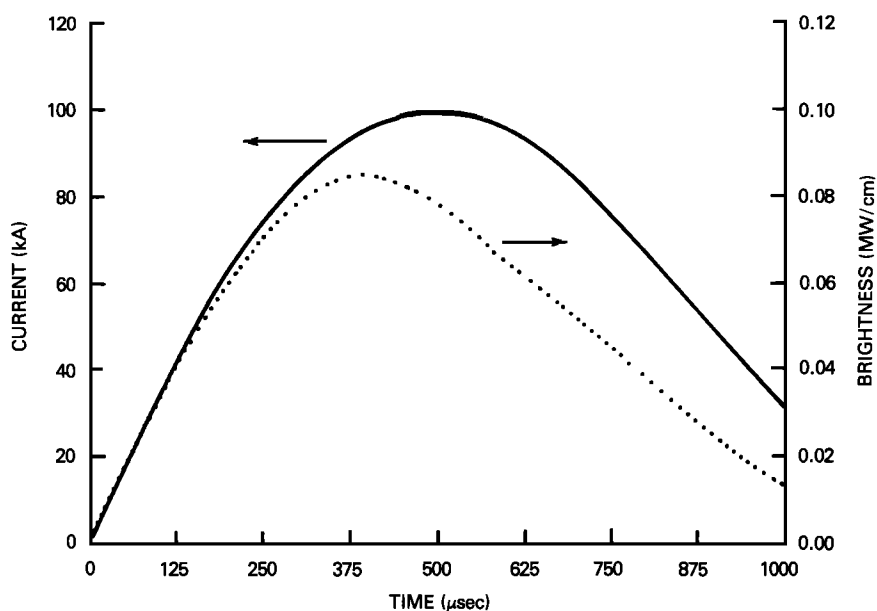


Fig. 10. Brightness with the LS-700 filter set and current for a 2-ms period, 100-kA discharge of bank 3.

dratic equation of the form

$$B = aI + bI^2 \quad (6)$$

was fit through the origin and through the regions of these two curves where the brightness varies slowly with current. Here B is the total radiation emitted into 4π sr in the wavelength interval of the LS-700 filter set, measured in units of 10^8 W m^{-1} of plasma column length, I is the discharge current in kiloamperes, and the constants a and b are 4.6119×10^{-4} and 4.0748×10^{-6} , respectively. Direct extrapolation using (6) predicts that a discharge with peak current of ~ 250 kA would produce a channel with peak brightness of $\sim 3.7 \times 10^7 \text{ W m}^{-1}$.

The uncertainty in the current measurement was limited to the readability of the oscilloscope trace, about $\pm 5\%$. The sensitivity of the photomultiplier and filter sets was determined using a calibrated tungsten lamp and was reproducible within $\pm 10\%$ throughout the experiment. Combining these uncertainties leads to an overall measurement uncertainty in the brightness versus current for the laboratory discharges of about $\pm 15\%$.

Time-integrated spectra covering the region from 3000 to 7200 Å were recorded for the 80-kA peak current discharge produced using bank 1 and the smoke aerosol. Emission lines of singly ionized nitrogen and oxygen predominate, with neutral nitrogen and oxygen lines present but considerably weaker. The H_α line at 6563 Å is also prominent at the red end of the spectrum. All through the visible region the line features are seen against a continuum background. This is entirely consistent with previous spectroscopic measurements of fast, Marx discharge-produced, air plasmas at NRL [Raleigh et al., 1981] and of natural lightning [Orville and Henderson, 1984]. There is no spectral evidence of migration of electrode material into the field of view during the short lifetime of this discharge, nor is there any evidence of emission by material from the aerosol particles.

Time-integrated spectra covering the region from 3000 to 7200 Å were also recorded for the 16-kA peak current discharge produced using bank 2 and the smoke aerosol. The

diameter of the discharge column is substantially larger than that of the bank 1 discharge, but the singly ionized nitrogen and oxygen lines emanate from only the very center of the luminous column corresponding to the narrow region heated by the initial, fast-ringing, Marx discharge. The brightest features of this spectrum emanate from neutral atomic and molecular species. Toward the ultraviolet end of the spectrum the CN molecular band appears. CN is not normally visible in natural lightning but has been seen when a continuously flowing current maintains a luminous channel between restrikes of a lightning bolt [Orville and Henderson, 1984]. H_α is again the brightest feature at the red end of the visible spectrum, with the neutral oxygen line at 7156 Å showing up in the near-infrared. Overall, this spectrum is very similar to that shown

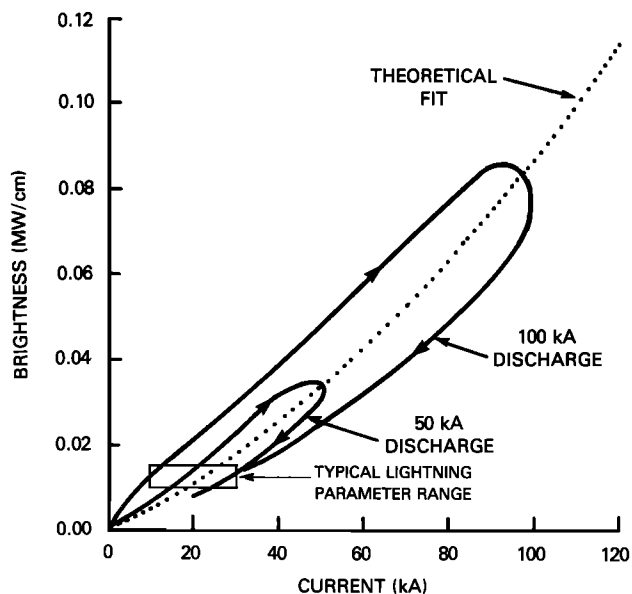


Fig. 11. Plot of brightness with the LS-700 filter set versus current for 50-kA and 100-kA discharges of bank 3. The region enclosed by the box indicates the range for current and brightness of typical natural lightning strikes.

in Figure 12 and quite different from that of natural lightning.

The spectral region under investigation was extended into the infrared to 8800 Å for the high-current discharges. Figure 12 presents four annotated, time-integrated spectrograms of the region 4600–8000 Å for the 100-kA peak current discharge produced by bank 3 with smoke aerosol. The molecular bands of CN in the ultraviolet (not shown) and of water vapor in the red are very distinct. Again, the lines from singly ionized atomic nitrogen and oxygen are emitted from only the small region heated by the Marx discharge, indicating that the bulk of the plasma column is relatively cool. Faint copper lines give the first evidence that a small amount of electrode material has migrated the required 50 cm, while the column was still luminous, to intrude on the field of view of both the spectrometer and the PMT. The potassium resonance lines at 7665 and 7699 Å are produced by gunpowder aerosol particles that have been heated within the bulk of the plasma column. The features in the near-infrared originate almost entirely from neutral oxygen and nitrogen atoms with a few argon lines from the naturally occurring 0.9% component of the atmosphere.

Spectra for the 50-kA peak current discharge produced using bank 3, but in which a water mist provided the aerosol particles required for laser initiation of the discharge, are quite similar to those of the 100-kA discharge (Figure 12). There was increased emission from water vapor and from neutral hydrogen (H_β and H_γ both became visible), while the CN band structure disappeared. Since water mist was not as effective as smoke particles for breakdown initiation, the electrode separation was reduced to 50 cm, with a commensurate increase in the contamination of the plasma column with copper and zinc from the electrodes.

4. DISCUSSION

For discharges with peak currents $\lesssim 100$ kA and rise times of ~ 0.5 ms, i.e., current rate of rise $\lesssim 200$ kA ms $^{-1}$, it is clear that interpolation using (6) would give a reasonable estimate (about $\pm 25\%$) of the peak brightness, and the uncertainty would be largely due to the variation of discharge brightness for the same current, as seen in Figure 11. But for the prominent NEIL channel at IVY-MIKE (Figure 4) the peak-measured brightness was $\sim 3.5 \pm 1.8 \times 10^7$ W m $^{-1}$, and the brightness rose continuously over a period of ~ 5 ms (from ~ 2.5 ms after detonation to ~ 7.5 ms). No simple expression exists that relates channel current, temperature, and brightness, or even attempts to allow for the effects of channel cooling. Therefore we must look for approximate relations that will allow extrapolation of the laboratory data to the NEIL conditions. First, we notice that during the first millisecond of its life the NEIL channel behaved very similarly to the laboratory discharge channels; thus at a time of ~ 3.5 ms, when the brightness had reached $\sim 10^7$ W m $^{-1}$, we suggest that direct comparison is permissible. Unfortunately, while the Wratten-12/LS-700 filter set very closely matches the upper and lower bandwidth cutoffs of the photo-recording system used at IVY-MIKE, it is more sensitive in the region of H_α . Furthermore, there is a total uncertainty of almost a factor of 2 in the measured intensity. Combining these uncertainties, the current in the prominent channel (Figure 4) at IVY-MIKE at ~ 3.5 ms is estimated to be between ~ 75 and ~ 175 kA.

To go beyond this point, we notice that the conductivity of air does not vary substantially with temperature above $\sim 12,000$ K, nor does it vary significantly with pressure be-

tween 1 and 10 atm [Plooster, 1971]. Thus the rate at which energy is deposited (by ohmic heating) in the channel per unit length is

$$\dot{W} \sim \frac{I^2}{\pi R_f^2 \langle \sigma \rangle} \frac{2\pi R_e}{\lambda} \quad (7)$$

where $\langle \sigma \rangle$ is the average conductivity (~ 100 ohm $^{-1}$ cm $^{-1}$), and the factor $2\pi R_e/\lambda$ assumes a helical distortion of the channel. Both R_e and λ increase with time, so that their ratio is nearly constant and, as seen in Figure 9, R_f is approximately constant. Thus

$$\dot{W} \propto I^2 \quad (8)$$

and the power balance equation becomes

$$\dot{W} \sim L_{\text{cooling}} + L_{\text{radiation}} \quad (9)$$

where L_{cooling} and $L_{\text{radiation}}$ are the energy loss rates due to turbulent convective mixing and radiation, respectively. Turbulent convective mixing causes cooling by mixing cold gas into the hot channel. The rate at which cold gas is mixed into the hot channel is $4\alpha/R_f^2$ vol/vol s $^{-1}$ [Greig et al., 1985], where α is the anomalous diffusivity and is given by

$$\alpha \sim \frac{c_s R_f}{66} \quad (10)$$

Here c_s is the ambient sound speed outside the channel. The cooling rate per unit length of channel is therefore

$$L_{\text{cooling}} \sim \frac{4\pi R_f c_s}{66} n_1 (3kT + X_D) \left(\frac{2\pi R_e}{\lambda} \right) \quad (11)$$

where n_1 is the ambient density around the current filament and X_D is the dissociation energy of nitrogen (~ 10 eV). This cooling rate is relatively independent of temperature because of dissociation. Thus we see that the radiative cooling rate must be at least approximately proportional to I^2 .

Another approach to the question of radiative cooling is to consider the mechanism of emission. The observed spectrum of the laboratory discharge channels consisted primarily of the spectrum of atomic nitrogen and atomic oxygen. This emission coefficient ϵ is proportional to the density of atoms n_A as

$$\epsilon \sim \frac{n_A \exp(-E/kT)}{Z(T)} \quad (12)$$

where E is the energy of the upper level of the transition and $Z(T)$ is the partition function [Drawin and Felenbok, 1965]. The emission per unit length of channel therefore becomes

$$B \sim \pi R_f^2 \frac{n_A \exp(-E/kT)}{Z(T)} \quad (13)$$

where we have averaged the emission coefficient over the radius, because for neutral atom line emission in air at atmospheric pressure the emission coefficient peaks at $\sim 15,000$ K and does not vary strongly with temperature over the range $\sim 12,000$ to $\sim 20,000$ K. The peak in the emission coefficient moves to higher temperatures as the pressure increases because of the variation of n_A [Burhorn and Wienecke, 1960], but the general behavior remains the same. Pressure balance requires

$$I^2 + 2\pi R_f^2 p_0 \sim 2\pi R_f^2 \sum nkT \quad (14)$$

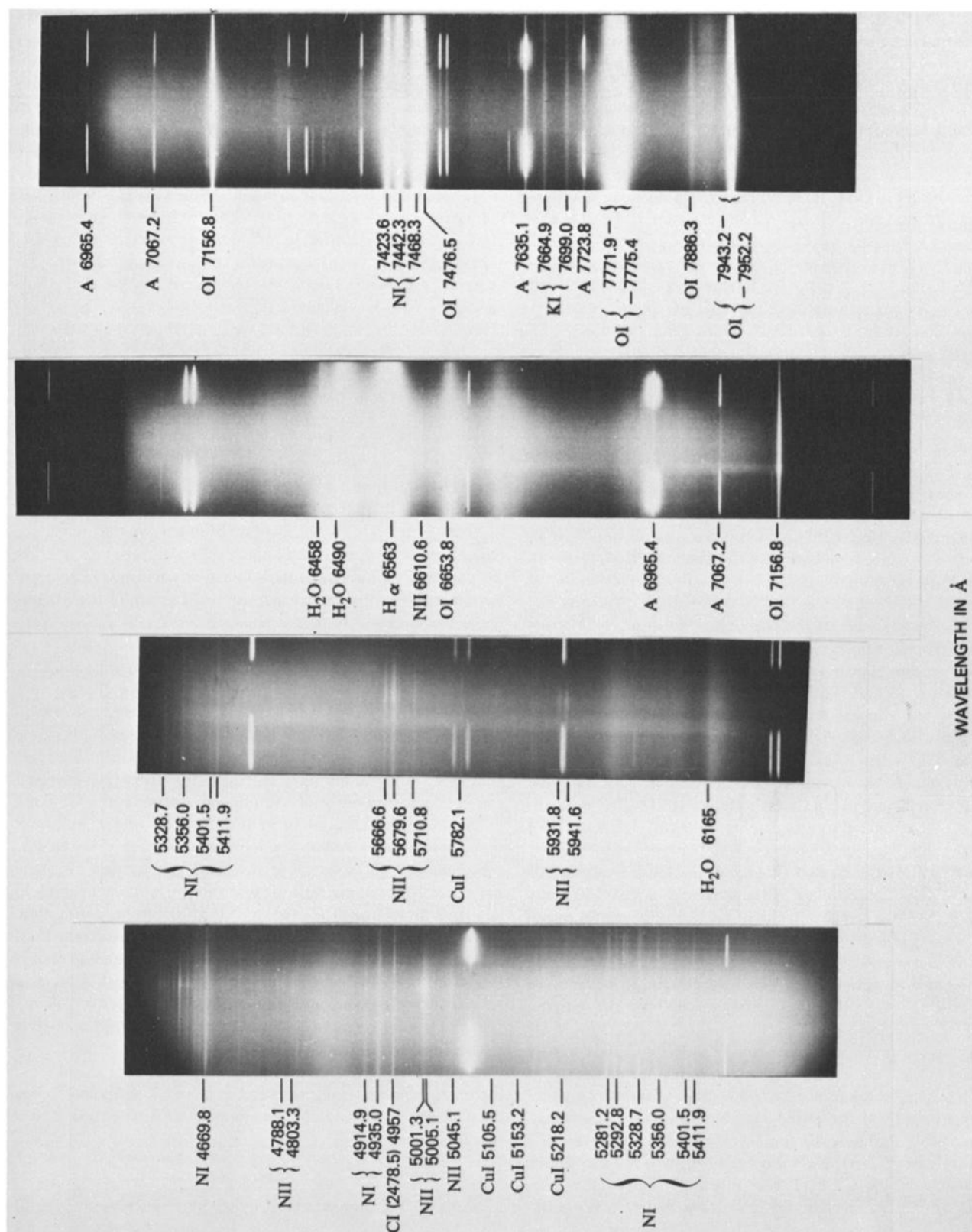


Fig. 12. Spectrum of a 2-ms period, 100-kA discharge of tank 3, with a smoke aerosol.

where p_0 is atmospheric pressure and $\sum n$ is the total particle density. Then, if temperature is approximately constant, so that n_A is a constant fraction of $\sum n$, we see that the atomic line emission is increasing because the total number of particles per unit length in the hot channel, $\pi R_f^2 \sum n$, is increasing with the magnetic pressure, which is proportional to I^2 .

These two different approaches are consistent and yield the same quadratic variation of $B(I)$ for temperatures, $kT \sim 1$ eV, which is itself consistent with the observed neutral atom spectrum (N I spectrum). The emission in the atomic ion line spectrum (N II spectrum) is $\sim 10,000$ times less than that in the neutral atom spectrum at $kT \sim 1$ eV, but is about equal to it at $kT \sim 2$ eV at atmospheric pressure. In deriving the variation of $B(I)$ we have assumed the line emission to be optically thin, which is the case for $kT \sim 1$ eV, radius $R_f < 10$ cm, and total pressures less than $\sim 10 p_0$, even if the lines are only Doppler-broadened [Griem, 1964; Wiese et al., 1966]. Thus there appears to be reason to believe that the quadratic dependence of brightness on current is more than fortuitous and that it is reasonable to extrapolate the experimental data, though it does depend on the rate of increase of the current in the discharge channel.

For times greater than ~ 3 ms, when the NEIL channels were observed [Uman et al., 1972], the observed rate of increase of the MIKE channel brightness is comparable to that of the 50-kA laboratory discharge, and thus we expect channel current to be reasonably well predicted by (6). Any deviation from this relationship is likely to be such that (6) results in an underestimate of the actual channel current, because (1) in Figure 11, if the brightness is not a quadratic function of the discharge current, it would have to be less than quadratic, i.e., closer to linear; and (2) for the longer-duration NEIL discharges, channel cooling will reduce the brightness of a given channel current. Because of the similarity of the laboratory and NEIL data and the limited nature of the extrapolation, we doubt that this would cause more than a 100% error. Thus we suggest that the peak current in the prominent NEIL channel is between ~ 200 kA, being the minimum obtained from the quadratic extrapolation, and ~ 600 kA. Here the sources of error are again the uncertainty in the absolute calibration of the MIKE photographic data ($\sim \pm 100\%$) and the uncertain difference in the relative sensitivity of the laboratory photo detection system and that used at MIKE (which leads to a probable underestimate of the current); in addition, there is the uncertainty in the extrapolation of the laboratory data to higher brightness (which also leads to a probable underestimate of the current).

We must now determine whether the discharge currents we have deduced for NEIL are compatible with the gamma output of the bomb itself. Uman et al. [1972] and Hill [1973] have both considered the quasi-steady state that exists shortly after detonation, in which the slow gamma flux maintains a nearly constant (on a millisecond time scale) Compton current density. Because of the radial gradient in the Compton current, negative charge is distributed in the atmosphere around the burst and electric fields are established. Both the charge density and the electric fields rise until the plasma return current σE removes charge at the same rate that it is being deposited by the Compton current. Hill [1973], scaling from the model calculations for a 20-kt burst given by Glasstone [1962], estimates values of the gamma flux, Compton current density, electric field, and conductivity at a time of 3 ms after time zero. In particular, Hill gives the source Compton current

density j_0 as $j_0 = 4 \text{ A m}^{-2}$, which, with his equation 10, gives a total Compton current into the upper half-plane of $0.83 \times 10^6 \text{ A}$ at 300 m and only $0.04 \times 10^6 \text{ A}$ at 1200 m. (The total source Compton current injected into the upper half-plane is more than $2 \times 10^6 \text{ A}$.) Thus using Hill's estimates, we conclude that a current of $0.8 \times 10^6 \text{ A}$ flows to ground between radii of 300 and 1200 m. At the same time, Hill [1973, p. 6356] points out that his estimates for the gamma flux are most likely a "lower limit" for IVY-MIKE, and we note that the Compton current scales directly with the gamma flux. Therefore we deduce that a total current of the order of $1 \times 10^6 \text{ A}$ (and possibly larger) flows to ground in the vicinity of the observed lightning channels. In very simple terms, the theory of Gardner et al. [1984] states that this "high pressure glow discharge" is unstable and tends to collapse into a few "arc channels" (a familiar problem to those using atmospheric pressure TEA CO_2 lasers). As they grow longer, these "arc channels" carry substantial fractions of the total "glow discharge" current, which funnels into the channel all along its length. Thus NEIL channel currents of ~ 240 kA are not obviously unrealistic. The total charge delivered to the base of the NEIL channel is approximately 2000 C, which is considerably larger than that delivered in natural lightning or that contemplated by Uman et al. [1972] and Hill [1973].

Finally, we consider the effect of MHD instabilities and channel cooling by turbulent convective mixing on the decay of the NEIL discharge channel. In previous work [Picone et al., 1981; Greig et al., 1985] it has been shown that turbulent convective mixing is a dominant process for cooling hot, reduced density channels in the atmosphere whenever there are asymmetries in the energy deposition. Certainly, the longer-period laboratory discharge channels exhibited grossly non-cylindrical energy deposition that was driven by MHD instabilities. These MHD instabilities grew to significant amplitude for the slow (millisecond time scale) laboratory discharges and, since the NEIL was of even longer duration, there is no reason to doubt that the NEIL discharge channels suffered the same behavior. In the first few milliseconds the current filament has radius R_f , and (7) and (11) represent the ohmic heating and the convective cooling of the channel, respectively. At these early times, channel cooling by turbulent convective mixing is much smaller than radiative cooling. Subsequently, as the current filament becomes more distorted, we suspect that the current will no longer flow around the spiral filament but will begin to jump from turn to turn. This represents a dramatic broadening of the current filament as the radius grows from R_f to R_c , a reduction in the magnetic pressure which prohibits recompression, and a reduction in the ohmic heating. It also results in increased cooling by turbulent convective mixing. Once this point is reached, convective cooling of the channel is dominant and simple estimates in which the internal energy ($3/2$ kT) of the hot channel of radius R_c is shared with the incoming cold gas suggest that the channel temperature can drop from $\sim 12,000$ K to less than ~ 4000 K in just a few milliseconds.

5. CONCLUSION

We have reexamined the original photographic records of IVY-MIKE, obtaining emission intensities for the luminous NEIL channels at different altitudes as functions of time. The absolute calibration for the IVY-MIKE records was deduced by comparison with the photographic records of other events of that era and the use of atmospheric data taken just prior to

the MIKE event. We find typical peak brightnesses of a few times 10^7 watts m^{-2} . Errors in the analysis lead to an uncertainty of $\pm 50\%$. Statistical errors arise mostly from scanning noise in the digitization process and from the averaging procedure used to obtain the specular density of each step of the step wedge. Atmospheric absorption is the largest potential systematic error, because the measured absorption for that day was unusually small. Corroboration with data taken on a second camera much closer to ground zero, however, supports a total error in the NEIL brightness measurements of a factor of 2.

In addition, we have created long arclike electric discharges in the atmosphere as a way of simulating the lightninglike phenomena (NEIL) that were observed at IVY-MIKE. Detailed spectroscopic analysis has shown that the plasma in these discharge channels consisted primarily of the natural constituents of atmospheric air, including typical ground-level impurities, but only trace quantities of electrode materials and materials used in the laser-guiding process. Furthermore, the intensity emitted per unit length of discharge channel, in the band pass 5000–7000 Å, which closely approximated the band pass of the cameras used at the IVY-MIKE test, was independent of the specific laser-guiding process, i.e., gunpowder smoke or water mist. For the long-duration discharges, in which the discharge channel was always in pressure equilibrium with the surrounding atmosphere, the channel brightness was also a simple function of the discharge current, within about $\pm 25\%$. Thus by direct comparison with the measured brightness of the NEIL channels, we have deduced that the peak current in the NEIL discharges was in excess of 200 kA. This value is consistent with recent theoretical estimates [Gardner et al., 1984; Fernsler, 1985] but is considerably larger than earlier estimates [Uman et al., 1972; Hill, 1973]. The accuracy of this determination of the NEIL discharge current is limited by the uncertainty of the equivalence of the filters used in these measurements and the response of the camera used at the IVY-MIKE test, by the uncertainty in the extrapolation of the laboratory data, and by the uncertainties in the NEIL channel brightness, to an overall accuracy of a factor of about 3. In fact, these errors are not simply statistical but lean in the direction to make this determination a lower bound, i.e., most likely the true current was higher, perhaps as high as 600 kA.

We have studied the structure of the laboratory discharge channels using time-resolved white light and schlieren photography. For the longer-duration discharges (approximately half-sine waves with half-periods up to 1 ms) the discharge channel was always in pressure equilibrium with the surrounding atmosphere, and the radius of the current channel was always significantly less than that of the density channel. In fact, although these discharges started as cylinders, MHD instabilities became a dominant feature of the current channel from about 40 μs onward. Thus at later times there was a current filament distorted by MHD instabilities whose amplitude was equal to or larger than the radius of the current filament, and this whole current structure resided inside the reduced density channel. Such a discharge channel inherently has a very nonuniform energy deposition profile and will therefore be cooled by turbulent convective mixing. Furthermore, the discharge channel has no stable equilibrium configuration. Thus we suggest that the observed decline of the NEIL luminous channels after ~ 10 ms is caused by rapid cooling of the discharge channel by turbulent convective

mixing, which follows an effective expansion of the current carrying channel driven by the MHD instabilities.

Acknowledgments. The authors gratefully acknowledge the assistance given by S. Hauver and E. Laikin of NRL and F. Bunker and A. Martinez of E. G. & G. We also acknowledge numerous discussions of this work with R. F. Fernsler of NRL and R. Gardner of MRC. In addition, one of us (J.D.C.) would especially like to thank the late Herman Hoerlin of Los Alamos National Laboratory and Conrad Longmire of Mission Research Corporation for the inspiration and guidance they provided in the early stages of this work. This work was supported by the Defense Nuclear Agency.

REFERENCES

- Barasch, G. E., Spectral intensities emitted by lightning discharges, *J. Geophys. Res.*, **75**, 1049, 1970.
- Brauer, F. L., and D. L. Hansen, f 2.9 Streak camera, *J. Opt. Soc. Am.*, **4**, 421, 1959.
- Buckner, J. K., Radiometric data reduction system for photographic film, *Rep. B-3660*, E. G. & G., Inc., Bedford, Mass., 1967.
- Burhorn, F., and R. Wienecke, Plasmazusammensetzung, Plasmadichte, Enthalpie und spezifische Wärme von Stickstoff, Stickstoffmonoxid und Luft bei 1, 3, 10 und 30 atm im Temperaturbereich zwischen 1000 und 30000°K, *Z. Phys. Chem. Leipzig*, **215**, 269, 1960.
- Carroll, J. S., *Photo Lab Index*, 24th ed., Morgan and Morgan, Inc., 1965.
- Constantine, B. J., Radiometric analysis of photographic data by the effective exposure method, *Rep. B-3768*, E. G. & G., Inc., Bedford, Mass., 1968.
- Curcio, J. A., L. F. Drummeter, C. C. Petty, H. S. Stewart, and C. P. Butler, An experimental study of atmospheric transmission, *J. Opt. Soc. Am.*, **43**, 97, 1953.
- Drawin, H. W., and P. Felenbok, *Data for Plasmas in Local Thermodynamic Equilibrium*, pp. 43, 277, Gauthiers-Villars, Paris, 1965.
- Fernsler, R. F., Analytical model of nuclear lightning, *Nav. Res. Lab. Memo. Rep. 5525*, Nav. Res. Lab., Washington, D. C., 1985.
- Gardner, R. L., M. H. Frese, J. L. Gilbert, and C. L. Longmire, A physical model of nuclear lightning, *Phys. Fluids*, **27**, 2694, 1984.
- Gilinsky, V., Kompaneets model for radio emission from a nuclear explosion, *Phys. Rev. A*, **137**, 50, 1965.
- Glasstone, S., *The Effects of Nuclear Weapons*, Rev. ed., p. 386. U.S. Atomic Energy Commission, Washington, D. C., 1962. (Reprinted as S. Glasstone, and P. J. Dolan, *The Effects of Nuclear Weapons*, 3rd ed., U.S. Department of Defense and Energy Research and Development Administration, Washington, D. C., 1977.)
- Greig, J. R., D. W. Koopman, R. F. Fernsler, R. E. Pechacek, I. M. Vitkovitsky, and A. W. Ali, Electrical discharges guided by pulsed CO₂ laser radiation, *Phys. Rev. Lett.*, **41**, 174, 1978.
- Greig, J. R., R. F. Fernsler, D. P. Murphy, R. E. Pechacek, J. M. Perin, and M. Raleigh, Laser guided electric discharges in the atmosphere, in *Proceedings of the 7th International Conference on Gas Discharges and Their Applications*, p. 464, Peter Peregrinus, London, 1982.
- Greig, J. R., R. E. Pechacek, and M. Raleigh, Channel cooling by turbulent convective mixing, *Phys. Fluids*, **28**, 2357, 1985.
- Greim, H. R., *Plasma Spectroscopy*, pp. 101, 173, McGraw-Hill, New York, 1964.
- Guo, C., and E. P. Krider, The optical and radiation field signatures produced by lightning return strokes, *J. Geophys. Res.*, **87**, 8913, 1982.
- Hill, R. D., Lightning induced by nuclear bursts, *J. Geophys. Res.*, **78**, 6355, 1973.
- Kompaneets, A. S., Radio emission from an atomic explosion, *Zh. Eksp. Teor. Fiz.*, **35**, 1538, 1958 (Sov. Phys. JETP, Engl. Transl., **8**, 1076, 1959.)
- Longmire, C. L., On the electromagnetic pulse produced by nuclear explosions, *IEEE Trans. Antennas Propag.*, **AP-26**, 3, 1978.
- Manheimer, W. M., M. Lampe, and J. P. Boris, Effects of surrounding gas on magnetohydrodynamic instabilities in Z-pinch, *Phys. Fluids*, **16**, 1126, 1973.
- Mitchell, C. K., F. J. Bunker, and F. Chavez, Calibration of 1952-vintage microfilm, *Tech. Memo. LAO-2730-1327*, E. G. & G., Inc., Los Alamos, N.M., 1984.
- Murphy, D. P., M. Raleigh, E. Laikin, J. R. Greig, and R. E. Pecha-

- cek, Electron beam transport through the atmosphere in reduced density current carrying channels, *9th International Symposium on Engineering Problems in Fusion Research*, vol. 2 p. 1548, Inst. of Elect. and Electron. Eng., New York, 1981.
- Orville, R. E., and R. W. Henderson, Absolute spectral irradiance measurements of lightning from 375 to 880 nm, *J. Atmos. Sci.*, **41**, 3180, 1984.
- Picone, J. M., and J. P. Boris, Vorticity generation by asymmetric energy deposition in a gaseous medium, *Phys. Fluids*, **26**, 365, 1983.
- Picone, J. M., J. P. Boris, J. R. Greig, M. Raleigh, and R. F. Fernsler, Convective cooling of lightning channels, *J. Atmos. Sci.*, **38**, 2056, 1981.
- Plooster, M. N., Numerical simulation of spark discharges in air, *Phys. Fluids*, **14**, 2111, 1971.
- Raleigh, M., J. R. Greig, R. E. Pechacek, and E. Laikin, Laser-initiated reduced density channels for transporting charge particle beams, *Nav. Res. Lab. Memo. Rep. 4380*, Nav. Res. Lab., Washington, D. C., 1981.
- Turman, B. N., Detection of lightning superbolts, *J. Geophys. Res.*, **82**, 2566, 1977.
- Turman, B. N., Lightning detection from space, *Am. Sci.*, **67**, 321, 1979.
- Turman, B. N., T. B. Cummings, and P. R. Deabenderfer, Measurement of optical power radiated by Florida lightning, *Rep. 76-7*, Air Force Tech. Appl. Cent., Patrick Air Force Base, Fla., 1976.
- Uman, M. A., D. F. Seacord, G. H. Price, and E. T. Pierce, Lightning induced by thermonuclear detonations, *J. Geophys. Res.*, **77**, 1591, 1972.
- Wiese, W. L., M. W. Smith, and B. M. Glennon, Atomic transition probabilities, vol. 1, *Nat. Stand. Ref. Data Ser., NSRDS-NBS 4*, 48, 1966.
- Wilson, D. C., The time dependent spectrum of IVY-MIKE (10.4 MT), *Rep. EGG-1183-5110*, E. G. & G., Inc., Los Alamos, N. M., 1980.

J. D. Colvin, Los Alamos National Laboratory, MS/E531 Los Alamos, NM 87545.

J. R. Greig, G-T Devices, 5705A General Washington Drive, Alexandria, VA 22312.

C. K. Mitchell, E. G. & G. Energy Measurements, Incorporated, P.O. Box 809, Los Alamos, NM.

D. P. Murphy, R. E. Pechacek, and M. Raleigh, Code 4751, Naval Research Laboratory, Washington, D. C. 20375.

(Received May 8, 1986;
revised February 4, 1987;
accepted February 5, 1987.)